Uncertainty evaluation of the atomic caesium fountain CSF1 of the PTB

S. Weyers, U. Hübner, R. Schröder, Chr. Tamm and A. Bauch

Abstract. A new primary frequency standard, the atomic caesium fountain CSF1, has been put into operation at the Physikalisch-Technische Bundesanstalt (PTB). ^{133}Cs atoms are cooled in a magneto-optical trap and in optical molasses. They are launched to a height of 39 cm above the microwave cavity centre. The resulting Ramsey resonance signal has a full-width half-maximum linewidth (FWHM) of 0.88 Hz. The first uncertainty evaluation yields a relative 1 σ frequency uncertainty of 1.4×10^{-15}. The short-term relative frequency instability of the CSF1 for averaging time τ is typically 3.5×10^{-13} $(\tau/\mathrm{s})^{-1/2}$, dictated by the available quartz oscillator as the local frequency source.

1. Introduction

By definition, International Atomic Time, TAI (Temps Atomique International) is a *coordinate* time scale, with the International System of Units (SI) second, as realized on the rotating geoid, as its scale unit. The realization of TAI is based on the Free Atomic Time Scale, EAL (Échelle Atomique Libre) computed at the Bureau International des Poids et Mesures (BIPM) as a weighted average of data obtained from about 210 atomic clocks – mainly commercial caesium clocks and a few hydrogen masers. A linear function of time is added to EAL with the slope adjusted in order to generate TAI as an international time reference conforming to the above definition. This so-called steering of TAI is based on comparisons between TAI and a few primary frequency standards that are operated in national metrology institutes and which realize the SI second with a specified uncertainty [1, 2].

During 1999 and 2000, data were available from the primary frequency standards NIST-7 (USA), CRL-01 and NRLM-4 (Japan), and JPO (France), which use optical pumping both for state selection and detection, and from the CS1, CS2, and CS3 of the PTB, which use magnetic state selection. In all these standards thermal atomic beams are used. Already in 1995 and 1996, the first atomic caesium fountain frequency standard using laser-cooled atoms was successfully operated at the Laboratoire Primaire du Temps et des Fréquences (BNM-LPTF, France). Its first published relative uncertainty estimate was 3×10^{-15}, which could later be reduced to 1.1×10^{-15} [3, 4]. Motivated by these outstanding results several metrology institutes worldwide initiated projects to construct caesium fountains. From the fountain NIST-F1 [5] of the National Institute of Standards and Technology (NIST, USA) first data were reported to the BIPM covering a period in November and December 1999, and first data of the fountain CSF1 of the PTB were reported for a period of 15 days in August 2000. A preliminary evaluation of the individual CSF1 uncertainty components had previously been performed [6, 7].

In the CSF1, laser-cooled caesium atoms are collected in a magneto-optical trap (MOT) and launched after a 100 ms molasses phase into a magnetically shielded titanium vacuum chamber. The atoms are launched to a height of 83 cm above the cooling region. During the ballistic flight, a TE011 microwave cavity mounted 44 cm above the MOT is passed twice. The atomic state is subsequently analysed in a detection region located between cavity and MOT. Ramsey fringes with a FWHM of 0.88 Hz are obtained. Frequency comparisons are made using two active hydrogen masers as local references. These masers in turn are compared with the PTB primary clocks and with UTC(PTB) and the results are reported to the BIPM. Thus the maser frequencies are known with respect to TAI for standard 5-day intervals. The CSF1 was compared with the masers following the same time schedule. The TAI scale unit could then be measured with respect to the SI second as realized with the CSF1, up to now in total during 60 days.

The design of the CSF1 is briefly outlined in Section 2, while Section 3 gives a detailed description of the individual uncertainty components. Some frequency measurement results are presented in Section 4 together

with the currently observed frequency instability, and conclusions are given in Section 5.

2. Fountain set-up

Figure 1 illustrates the mechanical design of the CSF1. The vacuum structure consists of the MOT region including the caesium reservoir at the bottom, the detection zone, all made from stainless steel, and the drift tube, made from titanium. The base pressure in the vacuum system is kept at a level of 10^{-7} Pa by a 200 l/s ion getter pump on top of the set-up. The atoms are trapped and cooled in a standard MOT set-up consisting of four laser beams in the horizontal plane, two vertical beams and a magnetic quadrupole field with a flux density gradient of 0.08 T/m at the trap centre. Typically, a number in the range of 10^7 caesium atoms is collected during a loading time of 0.3 s at a caesium background gas pressure of about 10^{-6} Pa. After the MOT magnetic fields are switched off, the atoms are further cooled to an equivalent temperature of 1.8 μK in a 100 ms molasses phase. The cold atoms, which are pumped during the cooling cycle into the $F = 4$ ground state level, are subsequently launched by a moving molasses [8].

Detection is performed using a scheme similar to that described in [3]. When the falling atoms cross a first transverse standing-wave light field tuned to the

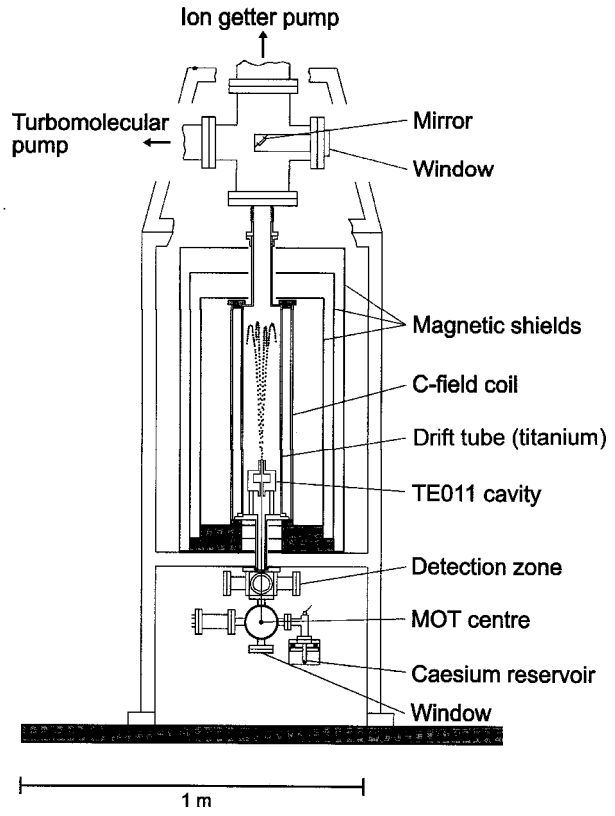

Figure 1. Mechanical design of the CSF1. MOT: magneto-optical trap.

$F = 4 \rightarrow F' = 5$ transition, each atom in the $F = 4$ state emits about 10^4 fluorescence photons. A fraction of approximately 2 % of the fluorescence light is imaged onto a photodiode. The time-integrated photodetector signal, N_4, is proportional to the number of atoms in the state $F = 4$. From the shape of the time-dependent photodetector signal one can infer the axial velocity spread of the atoms in the cloud, which indicates the corresponding kinetic temperature. The $F = 4$ atoms are then pushed away by a transverse travelling wave field tuned to the $F = 4 \rightarrow F' = 5$ transition. The atoms in the state $F = 3$ are detected in a lower-lying zone by a second standing-wave field, which consists of a superposition of light fields tuned to the $F = 3 \rightarrow F' = 4$ and $F = 4 \rightarrow F' = 5$ transitions. In this field the atoms are pumped to the state $F = 4$, and are detected by a second photodetector which yields a measure N_3 for the number of atoms in the state $F = 3$. The calculated fraction $N_{34} = N_3/(N_3 + N_4)$ indicates the fraction of atoms excited by the microwave field.

The laser-diode system [9] used for cooling and detecting the atoms is based on two extended-cavity diode lasers (ECDL). Using a lock-in technique, their emission frequencies are stabilized to the $F = 4 \rightarrow F' = 5$ and $F = 3 \rightarrow F' = 4$ saturated absorption signals of room-temperature Cs cells, respectively. Figure 2 shows a simplified overall optical scheme. The laser stabilized to the $F = 4 \rightarrow F' = 5$ transition is used as a master oscillator to injection-lock a 200 mW laser diode (slave), which provides the six cooling laser beams. The main part of the master laser light is used to detect the atoms. Light of the other extended-cavity diode laser repumps the atoms from the $F = 3$ ground state in the cooling and detection zones. The frequencies and intensities of the laser beams are controlled by acousto-optical modulators, which are also used in combination with mechanical shutters to switch off the laser beams in the time between launching and detection.

The design of the microwave cavity, which was described in detail previously [10, 11], was motivated by the need of both large apertures for the atomic passage and a small dependence of the phase of the microwave field on the position of the atomic trajectories. As in other fountains, the microwave transitions are therefore induced in a cylindrical cavity in which the magnetic field oscillates in the TE011 mode. This mode exhibits a high intrinsic quality factor, implying a small variation of the field phase with radial position in the cavity. Figure 3 shows a transverse section of the CSF1 microwave cavity and of the coupling waveguide structure. Phase variations are further reduced by symmetric coupling at opposite sides of the cylindrical cavity walls. The coaxial line carrying the microwave signal is tightly coupled with a waveguide that splits into two bent branches. The coaxial cable feed is shifted from the symmetry plane by $\lambda_g/4$ (λ_g, length of the guided wave) in order to excite the field of the cylindrical cavity with equal

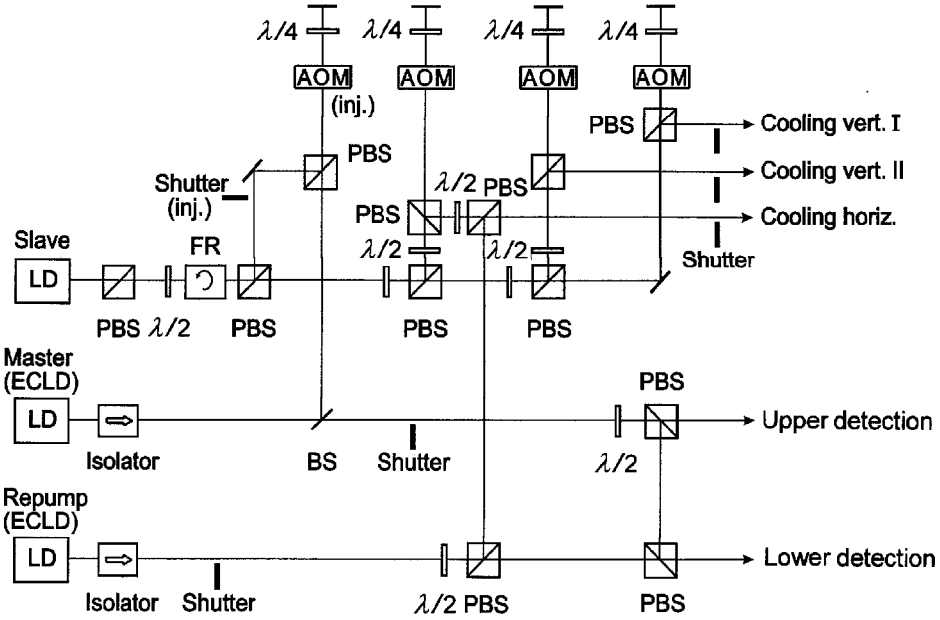

Figure 2. Simplified scheme of the laser system used for cooling, launching and detecting atoms. AOM: acousto-optical modulator; BS: beam splitter; ECLD: extended-cavity laser diode; FR: Faraday rotator; PBS: polarizing beam splitter. The laser light is guided to the fountain by polarization-maintaining optical fibres (not shown). The horizontal cooling light is split into the four horizontal cooling laser beams behind the optical fibre.

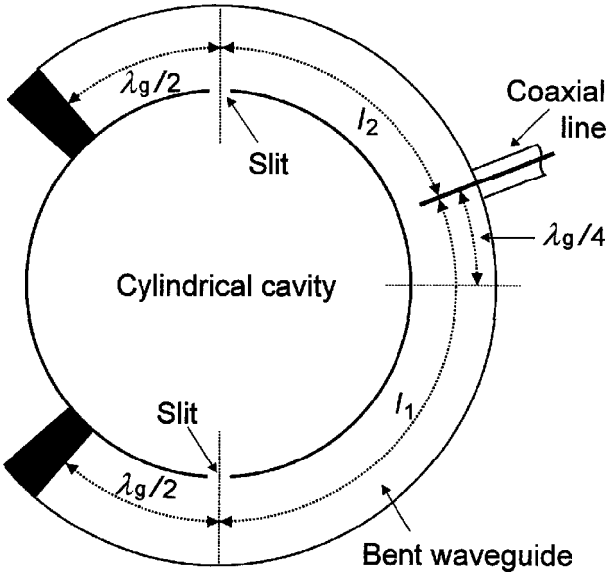

Figure 3. Schematic diagram of the microwave cavity for Ramsey excitation. The atoms pass through the centre of the cylindrical cavity, vertical to the paper plane. The cavity is excited by two mutually coupled bent waveguides fed by a coaxial line. λ_g is the length of the guided wave. $l_1 \approx 5\lambda_g/4$; $l_2 \approx 3\lambda_g/4$.

phase at the two symmetrical coupling slits. Because the two branches are not decoupled from each other, in the loss-free case a pure standing field is excited in the coupling waveguides and in the cavity. As a result, the dependence of the phase on the location vanishes even if the mechanical realization is slightly asymmetric. This implies that a rather strong coupling can be chosen. In our case the loaded cavity quality factor is 2000. In practice, losses are inevitable, but for the chosen design the phase dependence will still remain small [10, 11]. As a result of the strong coupling, the influence of temperature changes of the cavity on the microwave field amplitude in the cavity is sufficiently small so that the cavity temperature does not need to be actively stabilized, as the CSF1 is operated in a temperature-stabilized room (see Section 3.3). Cut-off tubes 7 cm in length and 1 cm in diameter are attached to the entrance and exit bores of the cavity to prevent microwave leakage from the cavity.

An additional state selection cavity [3] which was recently installed below the TE011 cavity is not shown in Figure 1. All data discussed in this contribution were taken either before its installation or without making use of it.

Figure 4 illustrates the synthesis of the microwave interrogation field from a low-noise BVA voltage-controlled quartz oscillator (VCXO, Oscilloquartz 860711) and the servo loop to control the oscillator frequency. The signal of the oscillator at $f_{\mathrm{n}} = 5$ MHz is multiplied to 9.2 GHz and mixed with the signal of a dielectric resonator oscillator (DRO) [12]. The beat signal is mixed with the signal of a commercial high-resolution frequency synthesizer locked to the same quartz oscillator. The output of the mixer is used to phase-lock the DRO, whose output frequency is the interrogation frequency f_{P}.

In the frequency measurement mode, the output frequency of the synthesizer is square-wave modulated (full-width $2w$) so that the central Ramsey fringe is probed on opposite sides during subsequent fountain cycles. The signal-processing electronics (detailed

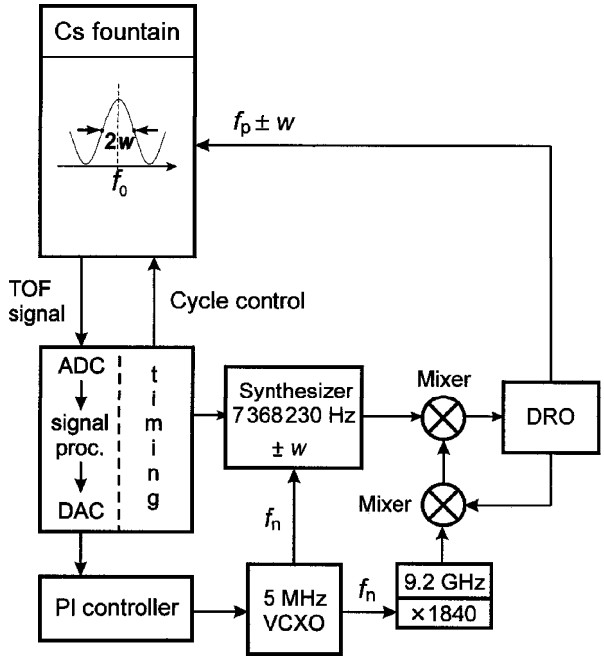

Figure 4. Overall schematic diagram of the fountain system. The frequency of the 5 MHz voltage-controlled quartz oscillator (VCXO) is locked to the atomic resonance of the fountain. A computer controls the timing for the cycle and processes the time-of-flight (TOF) signals. ADC: analogue-to-digital converter; DAC: digital-to-analogue converter; DRO: dielectric resonator oscillator.

description in Section 3.7) delivers a control voltage which is fed to the quartz oscillator so that the probing frequency is stabilized to the real fringe centre frequency. This differs from $f_0 = 9\,192\,631\,770$ Hz, the unperturbed caesium hyperfine transition frequency, by the sum of all systematic frequency shifts. In routine operation, the difference is well below 0.001 Hz, and its determination is the subject of Section 3. Thus the difference shows up directly in the quartz output frequency which is compared with that of the PTB hydrogen masers using a commercial phase comparator. The instability introduced by the measurement system is lower than the combined instability of the CSF1 and the masers by at least a factor of 5 for all employed averaging times τ. In a hold-over mode, the quartz can be phase-locked to an external 5 MHz reference signal in order to measure the Zeeman frequency (see Section 3.1) or to record Ramsey fringes.

3. Evaluation of frequency corrections F_i and their uncertainties

In this section the major frequency corrections and the corresponding contributions to the CSF1 standard frequency uncertainty are discussed as they have been evaluated to date. The evaluation should be considered as valid only in the CSF1 routine operation mode (explained below) used for the measurement of the TAI scale unit. For an exhaustive theoretical treatment of the frequency shift effects investigated the reader is referred to [13].

3.1 Magnetic field

Typically, the dominant frequency correction in caesium frequency standards is the frequency shift due to the static magnetic "C-field", which is applied in order to remove the degeneracy of the magnetic substates. This field increases the clock transition frequency by $f_C = 0.0427$ Hz $(B_C/\mu\mathrm{T})^2$, where B_C is the magnetic flux density of the C-field. The determination of the relative frequency correction $F_C = -f_C/f_0$ and its uncertainty is based on experimental data on the mean C-field strength, its inhomogeneity, and its temporal stability.

In the CSF1 an axial static magnetic field is produced by a long coil that is supported by an aluminium cylinder enclosing the titanium vacuum chamber. At the top and bottom of the chamber several compensation coils are mounted in order to extend the region of low magnetic field inhomogeneity. F_C is determined from a measurement of the Zeeman frequency f_Z, i.e. the separation between the $(F = 4,\ m_F = 1) \rightarrow (F = 3,\ m_F = 1)$ and the $(F = 4,\ m_F = 0) \rightarrow (F = 3,\ m_F = 0)$ hyperfine transitions, according to

$$F_C = -8\,(f_Z/f_0)^2 \quad \text{and} \quad \delta F_C = -16\, f_Z\, \delta f_Z / f_0^2, \tag{1}$$

where δf_Z represents a small variation of f_Z [13].

An atomic fountain makes it possible to map the C-field by launching the atoms to different heights h and determining f_Z for each height [3]. When recording f_Z as a function of h, special care has to be taken to avoid any misinterpretation of the Ramsey fringes [14, 15]. From $f_Z(h)$ the magnetic flux density $B_C(h)$ was calculated along the atomic trajectories. Figure 5 shows the result obtained after homogenization of the magnetic field by proper adjustment of the compensation coil currents. At a launch height of 83 cm, typically $f_Z = 700.1$ Hz (mean magnetic flux density $B_C = 0.1$ μT) is obtained, and, according to (1), a correction $F_C = -46.4 \times 10^{-15}$ is applied. From the data shown in Figure 5 the inhomogeneity of the magnetic flux density for the maximum launch height of 83 cm was determined as 0.16 nT (rms), only 0.16 % of the mean value. As a result, the uncertainty contribution due to the inhomogeneity of the C-field is negligible ($\approx 10^{-19}$). Temporal variations of f_Z did not exceed ±0.2 Hz over periods of months. Even if these remain undetected an uncertainty contribution of less than 3×10^{-17} according to (1) is the result.

3.2 Collisional shift

In the CSF1 the atoms are launched in the state $F = 4$ at a temperature of about 1.8 μK. In this case, collisions between cold caesium atoms are dominated by s-wave

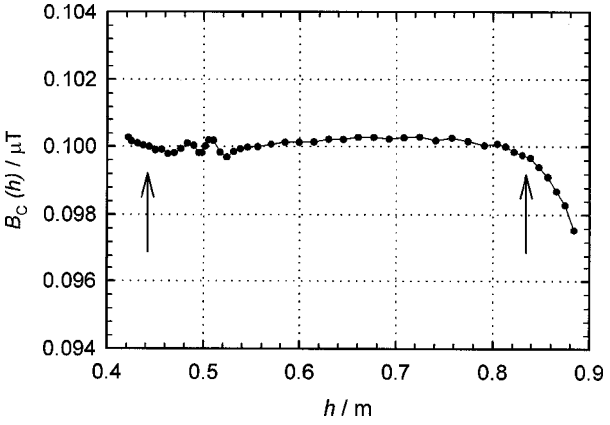

Figure 5. Variation of the magnetic flux density $B_C(h)$ along the drift tube in and above the microwave cavity. h is the height above the centre of the MOT. The arrows at 44 cm and 83 cm indicate the position of the centre of the cavity and the launch height used in the routine operation mode, respectively.

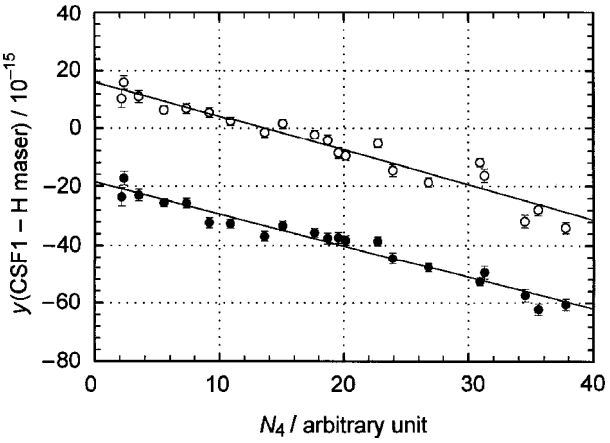

Figure 6. Relative frequency differences y(CSF1 – H maser) between the CSF1 and the hydrogen masers H1 (solid circles) and H2 (open circles) of the PTB as a function of the average number of detected atoms N_4. The vertical error bars reflect the statistical uncertainty arising from the CSF1 noise and the noise of the hydrogen masers. Solid lines represent linear least-squares fits to the data points. The frequency differences are corrected for F_C and F_G (see Sections 3.1 and 3.10).

scattering and the collisional shift depends linearly on the mean density $\overline{n}$ of the atomic cloud between the two microwave interactions [16, 17]. The collisional frequency shift can be obtained by determining $\overline{n}$ and relying on published frequency shift coefficients [17]. In order to avoid the intricacies of an absolute density measurement as well as of a modelling of the cloud expansion during the ballistic flight, we determine the collisional shift by measuring only relative densities. If the experimental conditions such as detection efficiency, launching height, and atomic temperature are kept constant, the signal N_4 of detected atoms in the state $F = 4$ is proportional to $\overline{n}$. Thus, a linear dependence of the fountain frequency on N_4 is expected, and the unperturbed frequency can be obtained by extrapolation to signal $N_4 = 0$.

In a series of measurements, N_4 was varied using different MOT loading times (0.2 s to 1.6 s) and caesium background gas pressures. The results of frequency measurements between the CSF1 and two local active hydrogen masers are depicted in Figure 6 as a function of N_4. Each data point typically represents a 19-hour average and was plotted at the corresponding average $\langle N_4 \rangle$. The shot-to-shot variations of N_4 were typically less than 2 %; on some occasions N_4 changed slowly by about 5 % in total. The masers exhibited a relative frequency drift of the order of 10^{-16}/day (see Section 4). To avoid systematic errors arising from the frequency drift of the masers, the data were collected using a random sequence of $\langle N_4 \rangle$ values in the range between 2 and 38. The results confirm the expected linear dependence of the observed frequency differences on N_4. The solid lines in Figure 6 indicate linear least-squares fits to the data with resulting slopes of $m_{H1} = -(1.09 \pm 0.05) \times 10^{-15}$ and $m_{H2} = -(1.18 \pm 0.08) \times 10^{-15}$. Calculating the weighted average of both slopes yields $-(1.12 \pm 0.04) \times 10^{-15}$. The residuals from the linear regressions exhibit Gaussian distributions.

The slope m is determined periodically to gain more experience about its constancy. Frequency differences between the CSF1 and the two masers are measured while operating CSF1 alternately at low and high atomic density (typically corresponding to $N_4 \approx 9$ and $N_4 \approx 30$) during several days. A further five slope determinations have been performed to date, which have yielded a mean slope of -0.887×10^{-15}. The scatter of the individual measurement results around the mean is within $\pm 0.09 \times 10^{-15}$. Only the result of the earliest slope determination significantly deviates from this mean. This is thought to be due to the fact that at the time of the first measurement the final residual gas partial pressure in the cavity region was not yet reached. An increased rate of collisions of the falling atom cloud with background gas molecules in the cavity region and below caused fewer atoms to be detected from a cloud of the same mean density $\overline{n}$. This would explain a larger collisional shift at a certain number N_4 of detected atoms and thus explain the larger slope in the data shown in Figure 6.

When data are collected for contributing to TAI, the CSF1 is operated in a so-called routine operation mode at $N_4 \approx 9$. This represents a compromise between low instability and low uncertainty owing to the collisional frequency shift. During the measurement, N_4 is recorded and the relative frequency correction is afterwards calculated based on the average $\langle N_4 \rangle$ and the average slope determined before and after a routine measurement. We typically obtain a relative frequency correction of $F_{coll} = 8.0 \times 10^{-15}$.

The uncertainty of the correction F_{coll} is made up of two components. The first reflects a possible undetected change of the proportionality factor between N_4 and $\overline{n}$ of as much as 10 % during the routine measurement

interval. The results obtained so far indicate that for otherwise unchanged experimental parameters this is a conservative estimate. The second is due to the statistical uncertainty of the slope determination, mainly caused by the long-term instability of the masers. Typically the square root of the quadratic sum of both components yields a relative frequency uncertainty contribution of 1×10^{-15}. This uncertainty contribution is larger if the CSF1 is not in routine operation. It might be reduced by more detailed studies of the collisional frequency shift under various experimental conditions, in particular by use of the state selection cavity in the future. A more stable reference in the long term, such as a second fountain frequency standard, could reduce the statistical uncertainty of the slope determination.

The condition $N_4 = 9$ corresponds to a number of detected atoms of about 2×10^5, as deduced from a signal-to-noise measurement [15]. Based on the LPTF results [17], a frequency shift of $F_{\mathrm{coll}} = 8.0 \times 10^{-15}$ corresponds to an average density $\overline{n} \approx 8.0 \times 10^6/\mathrm{cm}^3$, which is in reasonable agreement with the value of $\overline{n}$ that is estimated from the CSF1 signal without precise knowledge of the atomic cloud size.

3.3 Black-body shift

The fountain is placed in the PTB clock hall whose temperature is stabilized to 296.7 K, with peak-to-peak variations of ±0.2 K for 95 % of the time. The atoms are shielded during their ballistic flight against both ambient light in the clock hall and stray light from the optical table. Thus they are subjected only to thermal radiation of the vacuum enclosure. We assume that this radiation gives rise to a spectral power density distribution which is equivalent to that of a black body. Three Pt-100 resistances are mounted along the titanium drift tube. The absolute uncertainty of the temperature measurement using the Pt-100 resistances is 0.3 K. The temperature gradient along the cylinder, indicated by the Pt-100's, is between 0.1 K and 0.3 K. Typically the bottom is slightly warmer than the top because of heat generated in the MOT coils. During 2000, each of the indicated temperatures remained stable to within 0.2 K with an unchanged temperature gradient. According to [18], the clock transition frequency is shifted by

$$f_{\mathrm{acs}} = -1.573(3) \times 10^{-4}\,\mathrm{Hz}\,(T/300)^4 \times [1 + 0.014\,(T/300)^2] \qquad (2)$$

in the presence of thermal radiation from a black body at temperature T. Hence, taking into account the mean temperature of 297.0 K of the CSF1 drift tube and the cavity, a relative frequency correction of 16.7×10^{-15} is applied. Taking into account potential radial temperature gradients and possible deviations from an ideal black-body characteristic due to the unknown emissivity of the titanium chamber, we assume a relative frequency uncertainty contribution of 0.2×10^{-15}, which corresponds to an uncertainty of the temperature of about 1 K.

3.4 Majorana transitions, Rabi pulling, Ramsey pulling, microwave leakage

In order to avoid Majorana transitions [19], an arrangement of axial correction coils prevents zeroes and abrupt changes of the magnetic field along the path of the atoms between MOT and microwave cavity. In the CSF1 the population difference in the state $F = 4$,

$$A = \frac{N\,(m_F = +1) - N\,(m_F = -1)}{N\,(m_F = 0)}, \qquad (3)$$

has been reduced to less than 5 % by careful adjustment of the polarization state of the vertical molasses beams. A calculation of Rabi pulling [13] for $A = 20$ % predicts a shift of less than 1×10^{-17} at optimum microwave excitation (π pulse for the clock transition). No calculations have as yet been made for the potential magnitude of Ramsey pulling [20]. From previous studies it is known, however, that frequency measurements for various microwave field strengths could reveal the presence of such shifts without making it possible to distinguish between them [21, 22]. Experimental studies showed that even when A was as large as 30 % and the microwave power was increased by a factor of 9 with respect to the optimum value, the frequency shift remained below 2×10^{-15}, the measurement uncertainty being determined by the long-term instability of the reference maser frequencies. Based on these findings, the current estimate for the frequency shifting effect of Rabi and Ramsey pulling, Majorana transitions, and microwave leakage in normal operation is less than 0.5×10^{-15}. Further studies are planned when the use of the state-selecting microwave cavity will allow populating individual m_F levels.

3.5 Cavity-related shifts: residual first-order Doppler effect and cavity pulling

A general advantage of an atomic fountain microwave frequency standard is that the atoms cross the same microwave cavity twice. If the atomic trajectories were perfectly vertical, frequency shifts due to axial and radial cavity phase variations would be perfectly cancelled as each atom would interact with the field once with velocity v (upwards) and once later with $-v$ (downwards). It is the transversal residual thermal velocity and a possible misalignment of the launching direction that cause a spread of the trajectories between the first and second passage through the cavity. In this case, a non-vanishing transverse phase variation of the cavity field can give rise to a residual first-order Doppler-effect frequency shift, unless the trajectories are distributed around the vertical symmetry axis in a proper way.

The microwave field in the cavity can be described as a superposition of various field modes that are excited with different amplitudes and phases. In the CSF1 cavity design (see Figure 3) a single microwave feed excites two symmetrically arranged vertical coupling slits [10, 11]. For exactly symmetric coupling, transverse electrical field modes TEn11 with $n = 0, 2, 4, \ldots$ can be excited in the cavity, but the field modes TEn11 with $n = 1, 3, \ldots$ are suppressed. Hence the predominant first-order Doppler shift contribution results from the TE211 mode. If one assumes in a worst-case estimate that all atoms ascend in a negligibly small cloud through the cavity centre and descend next to one of the coupling slits (still in a negligibly small cloud on one side of the cut-off bore), the residual relative first-order Doppler-effect frequency shift is calculated to be less than 0.5×10^{-15}.

For asymmetric coupling, further first-order Doppler-shift contributions are due to the TE111 mode and the TE311 mode. For a coupling asymmetry of 10 %, which is much larger than the asymmetry expected from mechanical tolerances, one calculates a residual relative first-order Doppler-effect frequency shift of less than 0.2×10^{-15}. This is another worst-case estimate, where it is assumed that all atoms ascend through the cavity aperture next to one coupling slit and descend again next to the other slit (again in a negligibly small cloud on one side of the cut-off bore upwards, on the opposite side downwards).

If the non-horizontal molasses laser beams are vertically well-aligned and centred to the microwave cavity axis and all laser-beam intensities are balanced, both cases considered here are improbable. Furthermore, the extension of the atomic cloud is non-negligible, so that all remaining effects are strongly averaged. A maximum relative frequency uncertainty of 0.5×10^{-15} is estimated. Further experimental and theoretical studies are planned in this respect.

On the other hand, by operating the fountain with a number of atoms of the order of 10^7 and using a cavity with a loaded quality factor of 2000, we are far from maser oscillation [13]. Therefore, at a potential detuning of 300 kHz and optimum microwave excitation, the frequency shift due to cavity pulling is calculated to be less than 10^{-18}, according to equation (5.6.123) of [13].

3.6 Time dilatation: relativistic Doppler effect

Special relativity predicts that due to time dilatation the clock frequency observed in the laboratory frame is reduced, and thus a correction $F_{\mathrm{D}} \approx \langle v^2 \rangle / (2c^2)$ has to be applied. In order to launch the atoms to 39 cm above the microwave cavity they are started with an initial velocity of 4.05 m/s. Simple calculation shows that the mean quadratic velocity of the atoms above the microwave cavity is $\langle v^2 \rangle = 2.57$ m^2/s^2. From this, one calculates a corresponding relative frequency shift contribution of -1.4×10^{-17}. This shift and the associated uncertainty contribution of much less than 10^{-17} are neglected here.

3.7 Electronics and microwave spectral impurities

This section summarizes the potential frequency shifts caused by spectral impurities of the interrogation signal and by faulty processing of the fluorescence signals, which yield the control voltage for the VCXO.

Calculations, based on the theory developed in [13], show that sidebands of the microwave interrogation field with frequency separations in the range of 50 Hz are the most efficient cause of a possible frequency shift. In the present set-up, such sidebands are suppressed by at least –60 dB relative to the carrier frequency. For a one-sided 50 Hz sideband at –60 dB and optimum microwave excitation, one calculates a maximum shift of 4.4×10^{-17}. Thus a corresponding relative uncertainty contribution of 0.1×10^{-15} is attributed, which is a rather pessimistic estimate, because the actual residual sideband structure is highly symmetric.

From cycle to cycle the synthesizer output frequency is switched between $f_0 + w$ and $f_0 - w$. In the fountain system there is no common frequency reference for the microwave frequency modulation and the synthesized microwave radiation. Phase fluctuations from the frequency synthesis (spurious signals) are not synchronous to the switching so that they are cancelled out [12].

From the digitized photodetector time-of-flight signals, indicating the populations of the level $F = 4$, N_4, and of the level $(F = 3, m_F = 0)$, N_3, the fraction $N_{34} = N_3/(N_3 + N_4)$ is calculated, which is almost independent of fluctuations of the total atom number. Differences between successive recordings of N_{34} are passed to a digital integrator whose output feeds a 12-bit digital-to-analogue converter (see Figure 4). Its output is fed to a PI-controller, which finally delivers the control voltage for the quartz. Dimensions were chosen such that the digital integrator handles the rapid fluctuations of the VCXO whereas the analogue integrator handles the constant fraction and the long-term variation of the necessary quartz control-voltage due to ageing. Systematic errors arising from a potential quadratic frequency drift of the VCXO and a linear drift of the offset of the operational amplifier in the analogue integrator are expected to contribute less than 0.1×10^{-15} in relative units. This estimate is based on experimental findings and the specifications of the individual components.

A potential source of systematic error could result from a reproducible and systematic variation of the efficiency to measure N_{34} from cycle to cycle. The layout of the electronic system was designed to avoid any cross-talk problems. On the other hand, a malfunction of one of the shutters (see next section), for example, might manifest itself only once every second cycle. Preliminary experimental investigations

did not reveal any malfunctions. In summary, no relative frequency uncertainty contribution larger than 0.2×10^{-15} is expected to arise from the electronics.

3.8 Light shift

The interaction of atoms with laser light during the ballistic flight in and above the microwave cavity entails a frequency shift through the ac Stark effect (light shift) [13]. To prevent this effect, the rf supply of the AOMs (see Figure 2) is switched off. The residual laser light is blocked by mechanical shutters in front of each optical fibre connecting the optical table and the fountain set-up. Furthermore, the injection locking of the slave laser is interrupted by a mechanical shutter (inj.) blocking the master laser light. Frequency measurements were performed alternately blocking or not blocking the residual light by this shutter. The results deviated by less than 2×10^{-15}, the measurement uncertainty being determined by the long-term instability of the reference maser frequencies. Based on these findings, the potential shift under standard conditions is estimated to be below 0.2×10^{-15}.

3.9 Background gas collisions

The residual gas partial pressure in the CSF1 is in the low 10^{-7} Pa range. In this pressure range, the estimated relative frequency shift due to collisions with background gas atoms and molecules is less than 0.5×10^{-15} [3].

3.10 Gravitational red shift

As the gravitational red shift is not significant for the realization of the *proper* second, it does not need to be included in the total uncertainty budget. However, knowledge of its value is important for comparisons with distant clocks and contribution to TAI. For the CSF1, the mean height of the atoms above the geoid during their ballistic flight above the microwave cavity centre is 80.1 m. A relative frequency correction of $F_{\mathrm{G}} = -8.7 \times 10^{-15}$ is thus applied, so that the clock frequency is realized as if the CSF1 would be operated on the rotating geoid. The relative uncertainty of F_{G} is of the order of 10^{-16}, which corresponds to an uncertainty of the height of 0.9 m.

3.11 Summary

Other frequency shifting effects (dc Stark shift, Bloch-Siegert shift [13]), which are estimated to be of the order of less than 10^{-17} in the case of the CSF1, are thus neglected here. In conclusion it can be stated that the main contributions to the CSF1 uncertainty are of the order of 1×10^{-15} or less and that they are linearly independent. Therefore the resulting standard uncertainty is the square root of the sum of squares of the individual components listed in Table 1 and amounts to 1.4×10^{-15} ($1\ \sigma$).

Table 1. Current uncertainty budget of the CSF1.

Effect	$10^{15} \times$ Correction	$10^{15} \times$ Uncertainty
C-field	–46.4	<0.1
Collisional shift	8.1	1
Black-body shift	16.7	0.2
Majorana transitions, Rabi pulling, Ramsey pulling, microwave leakage	–	0.5
First-order Doppler effect	–	0.5
Microwave spectral impurities, electronics	–	0.2
Light shift	–	0.2
Background gas collisions	–	<0.5
Total 1 σ uncertainty		1.4

4. Frequency measurement results

Frequency measurements were started on a regular basis in November 1999. During the first months, the main interest was in gathering the information required for a preliminary uncertainty evaluation [6, 7]. Later the state-selection cavity was installed. Frequency measurements, however, continued without it. Since August 2000 four measurement series have been performed during which the CSF1 contributed to the realization of TAI, each for a period of three standard 5-day intervals: MJD 51764-51778, MJD 51799-51813, MJD 51824-51838, MJD 51864-51878. Figure 7 depicts the corresponding relative frequency differences y(CSF1 – H1) between the CSF1 and the maser H1, which were communicated to the BIPM. The linear least-squares fit to the data points in Figure 7 indicates a frequency drift of maser H1 of $(0.137 \pm 0.009) \times 10^{-15}$/day. A similar result is obtained when comparing the H1 maser with the primary clock CS2, however with a considerably larger measurement uncertainty.

Measurement of the TAI scale unit with respect to the SI second as realized with the CSF1 has been possible with a relative combined uncertainty of 2.6×10^{-15}, as documented in Section 5 of *Circular T*, published by the BIPM Time Section [23]. Figure 8 shows the data of all primary frequency standards having contributed to TAI during the recent two-year period. The deviation found with the CSF1, NIST-F1 and NIST-7 is significant with respect to the comparison uncertainty, and steering of TAI has already been affected [23]. This steering can now be based on more accurate data than before.

As mentioned above, preselection of atoms in the substate $m_F = 0$ [3] has not yet been used in the CSF1. Hence the frequency instability is influenced by a substate partition noise contribution which reflects the statistical shot-to-shot fluctuation of the number of atoms in the respective substates (F, m_F) as described by the binomial distribution law [15]. With the optical

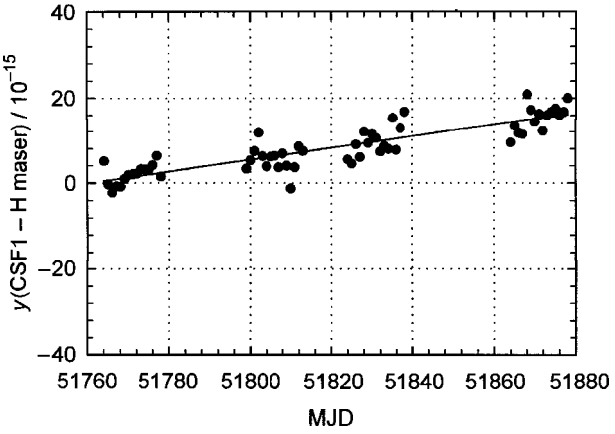

Figure 7. Relative frequency differences y(CSF1 – H1) between the CSF1 and the maser H1 corresponding to four measurement cycles (each of a period of 15 days), subsequently communicated to the BIPM. MJD designates the Modified Julian Day; MJD 51760 corresponds to 2000-08-04. All corrections were applied as described in Section 3. The solid line is a linear least-squares fit to the data and yields a drift of $(0.137 \pm 0.009) \times 10^{-15}$/day.

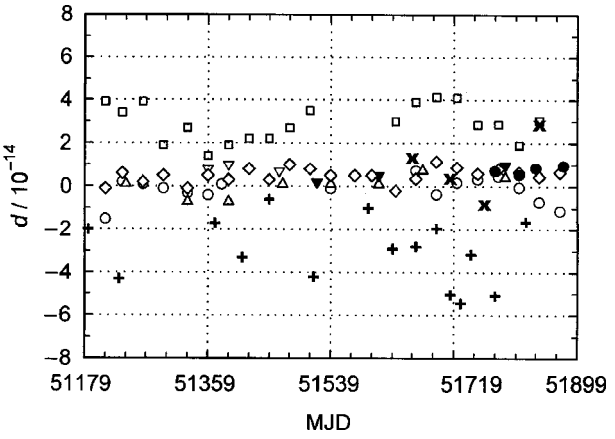

Figure 8. Fractional deviation d of the duration of the TAI scale interval from the SI second as realized by the individual primary frequency standards CSF1 (●), CS1 (○), CS2 (◇) and CS3 (□) of the PTB; NIST-7 (△) and NIST-F1 (▼) (USA); NRLM-4 (+) and CRL-01 (✖) (Japan); and JPO (▽) (BNM-LPTF, France), during the period MJD 51179-51879. MJD designates the Modified Julian Day; MJD 51179 corresponds to 1999-01-01.

detection system employed, photon shot noise is negligible, so that only the partition noise, quantum projection noise, electronic noise of the photodetector and local oscillator noise are of concern [6, 15]. Figure 9 illustrates the relative frequency instability, expressed by the Allan standard deviation $\sigma_y(\tau)$. Operating the CSF1 with a detected atom number of about 2×10^5 per cycle $\sigma_y(\tau) = 3.5 \times 10^{-13}\ (\tau/\mathrm{s})^{-1/2}$ is obtained. For averaging times $\tau > 20\,000$ s, the day-to-day frequency instability of the maser becomes apparent.

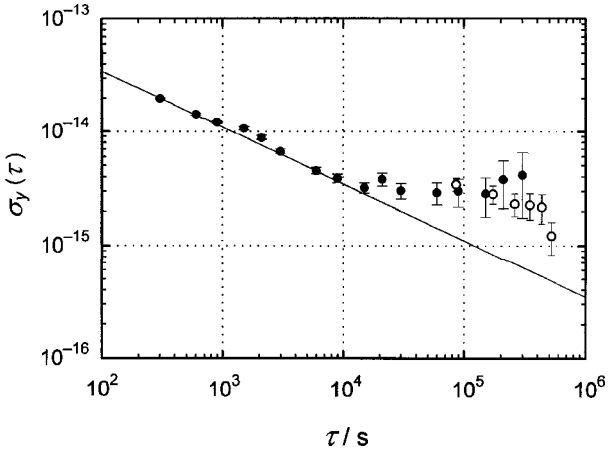

Figure 9. Allan standard deviation $\sigma_y(\tau)$ for averaging time τ of relative frequency differences y(CSF1 – H2) for operating the fountain with a detected atom number of about 2×10^5. Solid circles: data based on a representative subset of 15 days; open circles: data based on the 60-day period indicated in Figure 7. The straight line indicates an Allan standard deviation $\sigma_y(\tau) = 3.5 \times 10^{-13}\ (\tau/\mathrm{s})^{-1/2}$.

It was observed that increasing the number of detected atoms by increasing the MOT loading time did not reduce the instability, presumably due to local oscillator noise [3, 6, 15]. On the other hand, operating the CSF1 in the current configuration with an increased number of detected atoms would increase the uncertainty due to collisions. With preselection of atoms in the $m_F = 0$ substate, however, the number of launched atoms could be increased by a factor of 4 without increasing the collisional shift, assuming that 1/8 of the atoms are in the substate $m_F = 0$ [15, 17]. Using the currently available quartz oscillator in the microwave synthesis electronics, a frequency instability of the order of $\sigma_y(\tau) = 1.5 \times 10^{-13}\ (\tau/\mathrm{s})^{-1/2}$ can be expected without degrading the uncertainty value.

5. Conclusions

A first evaluation of the uncertainty contributions of an atomic fountain frequency standard developed at the PTB has been performed. Operating conditions providing an advantageous compromise between low uncertainty and low instability were identified. Even without preselection of atoms in the substate $m_F = 0$, a relative frequency uncertainty at the low level of 10^{-15} has been obtained. At the same time, the relative frequency instability is $\sigma_y(\tau) = 3.5 \times 10^{-13}\ (\tau/\mathrm{s})^{-1/2}$.

In the near future, the installed second microwave cavity will be used in order to preselect launched Cs atoms in the substate $(F = 3, m_F = 0)$ as described in [3]. The preselection allows the stability of the CSF1 to be further increased without increasing the collisional shift. In addition, the state preselection will allow a further reduction of some uncertainty contributions, in particular those arising from Rabi and Ramsey pulling.

Acknowledgements. The authors are very grateful to D. Griebsch for his commitment during the design, construction and operation of the CSF1 and to B. Fischer for his support in calculating the effect of microwave impurities in the CSF1.

References

1. Thomas C., Wolf P., Tavella P., Time Scales, *BIPM Monographie 94/1,* 1994.
2. Bauch A., Fischer B., Heindorff T., Hetzel P., Petit G., Schröder R., Wolf P., *Metrologia*, 2000, **37**, 683-692.
3. Clairon A., Ghezali S., Santarelli G., Laurent Ph., Lea S. N., Bahoura M., Simon E., Weyers S., Szymaniec K., *Proc. 5th Symp. Frequency Standards and Metrology*, Singapore, World Scientific, 1996, 49-59.
4. Laurent Ph., Lemonde P., Santarelli G., Abgrall M., Kitching J., Sortais Y., Bize S., Santos M., Nicolas C., Zhang S., Schehr G., Clairon A., Mann A., Luiten A., Chang S., Salomon C., In *Laser Spectroscopy* (Edited by R. Blatt, J. Eschner, D. Leibfried and F. Schmidt-Kaler), Singapore, World Scientific, 1999, 41-50.
5. Jefferts S. R., Meekhof D. M., Shirley J. H., Parker T. E., Levi F., *Proc. Joint Meeting 13th European Frequency and Time Forum – IEEE Int. Frequency Control Symp.*, 1999, 12-15.
6. Weyers S., Hübner U., Fischer B., Schröder R., Tamm Chr., Bauch A., *Proc. 14th European Frequency and Time Forum*, 2000, 53-57.
7. Weyers S., Hübner U., Schröder R., Tamm Chr., Bauch A., *CPEM 2000* book of abstracts, contribution MO2A-3.
8. Clairon A., Salomon C., Guellati S., Phillips W. D., *Europhys. Lett.,* 1991, **16**(2), 165-170.
9. Hübner U., Weyers S., Castellanos J., Griebsch D., Schröder R., Tamm Chr., Bauch A., *Proc. 12th European Frequency and Time Forum*, 1998, 544-547.
10. Schröder R., Hübner U., *Proc. 14th European Frequency and Time Forum*, 2000, 480-484.
11. Schröder R., Hübner U., Griebsch D., submitted to *IEEE Trans. Ultrason. Ferroelect. Frequ. Contr.*
12. Schröder R., *Proc 5th European Frequency and Time Forum*, 1991, 194-200.
13. Vanier J., Audoin C., *The Quantum Physics of Atomic Frequency Standards*, Bristol and Philadelphia, Adam Hilger, 1989.
14. Weyers S., Bauch A., Griebsch D., Hübner U., Schröder R., Tamm Chr., *Proc. Joint Meeting 13th European Frequency and Time Forum – IEEE Int. Frequency Control Symp*, 1999, 16-19.
15. Weyers S., Bauch A., Hübner U., Schröder R., Tamm Chr., *IEEE Trans. Ultrason. Ferroelect. Frequ. Contr.*, 2000, **47**(2), 432-437.
16. Tiesinga E., Verhaar B. J., Stoof H. T. C., van Bragt D., *Phys. Rev. A*, 1992, **45**(5), R2671-R2673.
17. Ghezali S., Laurent Ph., Lea S. N., Clairon A., *Europhys. Lett.*, 1996, **36**(1), 25-30.
18. Simon E., Laurent Ph., Clairon A., *Phys. Rev. A*, 1998, **57**(1), 436-439.
19. Bauch A., Schröder R., *Annalen der Physik,* 1993, **2**, 421-449.
20. Cutler L. S., Flory C. A., Giffard R. P., De Marchi A., *J. Appl. Phys.,* 1991, **69**(5), 2780-2792.
21. Bauch A., Fischer B., Heindorff T., Schröder R., *Metrologia,* 1998, **35**, 829-845.
22. Dorenwendt K., Bauch A., *Proc. Joint Meeting 13th European Frequency and Time Forum – IEEE Int. Frequency Control Symp.*, 1999, 57-61.
23. *Circular T*, Sèvres, Bureau International des Poids et Mesures, 2000-2001, issues 152-156, Sections 4 and 5.